PROCEEDINGS REPRINT

SPIE—The International Society for Optical Engineering

Reprinted from

Infrared Detectors and Focal Plane Arrays

18–19 April 1990
Orlando, Florida

Volume 1308

Invited Paper

Review of Schottky-Barrier Imager Technology

Walter F. Kosonocky

New Jersey Institute of Technology
Newark, NJ 07102

and

David Sarnoff Research Center
Princeton, NJ 08543-5300

ABSTRACT

This paper reviews the progress in the development of infrared image sensors with Schottky-barrier detectors. Schottky-barrier focal plane arrays (FPAs) are the only infrared imagers that are fabricated by the well established silicon VLSI process, therefore, at the present time they represent the most mature technology for large-area high-density focal plane arrays for many SWIR (1 to 3 μm) and MWIR (3 to 5 μm) applications. Infrared line sensing arrays with up to 4096 x 4 elements and 2048 x 16-TDI elements were developed and staring arrays with up to 512 x 512 elements have been reported. PtSi Schottky-barrier detectors (SBDs) represent the most established SBD technology for applications in the SWIR and MWIR bands at an operating temperature of about 80K. These SBDs can be designed for operation at 77K with a dark current density in the range of 1.0 to 4.0 nA/cm^2. Pd_2Si SBDs were developed for operation with passive cooling at 120K in the SWIR band. IrSi SBDs have also been investigated to extend the application of Schottky-barrier focal plane arrays (FPAs) into the LWIR (8 to 10 μm) spectral range. Because of very low readout noise, the IR-CCD imagers with PtSi SBDs which have quantum efficiency of .5% to 1% at 4.0 μm are capable of 300K thermal imaging with a noise equivalent temperature (NEΔT) from 0.04 to 0.15K for operation at 30 frames/s and f/1.2 to f/2.8 optics.

1.0 INTRODUCTION

In 1973, Shepherd and Yang of Rome Air Development Center (RADC), Hanscom AFB, MA proposed the concept of silicide Schottky-barrier detector (SBD's) focal plane arrays (FPAs) as much more reproducible alternative to HgCdTe FPAs for infrared thermal imaging [1]. Since then, the development of the SBD FPA technology progressed from the demonstration of the initial concepts in the 1970's [1-5] to the development of high resolution scanning and staring SBD FPAs in the 1980's that are now being considered for many applications for infrared imaging in the 1-3 μm (SWIR) and 3-5 μm (MWIR) spectral bands [6-65]. The progress in the development of the SBD FPAs is illustrated in Table 1 of Section 3. In the last 17 years RADC sponsored and guided most of the SBD FPA development in the United States. The first Pd_2Si [2], PtSi [2, 40, 25, 24, 58], and IrSi [28, 29] SBDs were made by RADC. RADC also has continued to make important contributions to the evaluation of performance and demonstration of high-quality thermal imaging with SBD FPAs [3-7, 17, 19, 20, 34, 42-44, 66-68]. The research organizations and companies involved in the development of the SBD FPAs included the David Sarnoff Research Center (Sarnoff) [3-7, 9-13, 21, 22, 39, 40, 48, 63-65], Mitsubishi [8, 14, 18, 23, 27, 37], Fujitsu [15], NEC [49, 59], Valvo [26, 39], Hughes [40, 54], EG&G Reticon [24, 25, 55], Loral Fairchild [50, 51], MIT Lincoln Laboratories [42, 44-46], Kodak [52, 53], and Ford Aerospace [58]. This paper[1] reviews the state-of-the-art of the SBD technology for scanning line-sensing and staring (area-sensing) SBD FPAs. With exception of the SWIR-band (1-3 μm) space-borne applications requiring passive cooling at temperatures above 110K for which Pd_2Si SBD were developed [10, 12, 22], the most advanced Schottky-barrier FPAs were developed

1 This paper represents an up-dated version of a similar review made by the author in 1987 [62].

Table 1. Reported Schottky-Barrier IR-CCD Focal Plane Arrays

Type of FPA	Pixel Size H x V $(\mu m)^2$	Fill Factor (%)	Type of SBDs Silicide	Ψ_{ms} (eV)	Year	Company	Ref.
25 x 50 IT	160 x 80	17	Thick-PtSi	0.27	1978	Sarnoff/RADC	3, 4, 5
			Thin-PtSi		1979	Sarnoff	6, 7
256 x 1	40 x 200	50-83	Thick-PtSi	0.27	1978	Sarnoff/RADC	4
			Thin-PtSi		1979	Sarnoff/RADC	6
32 x 63 IT	160 x 80	25	PtSi	0.208-0.22	1981	Sarnoff	13
			Pd_2Si	0.337	1982	Sarnoff	10, 12
64 x 128 IT	133 x 80	22	PtSi	0.208-0.22	1983	Sarnoff	9, 11
32 x 64 IT	133 x 80	19	PtSi	0.277	1981	Mitsubishi	8
64 x 64 IT Meander-Channel	130 x 70	23	PtSi	0.23	1983	Fujitsu	15
256 x 256 IT	37 x 31	25	PtSi	0.26	1983	Mitsubishi	14
64 x 64 MOS (1T)	80 x 65	56	PtSi	0.23	1983	Mitsubishi	18
160 x 244	80 x 40	39	PtSi	0.22	1984	Sarnoff	21
512 x 2	30 x 30	70-87	Pd_2Si	0.375	1985	Sarnoff	22
1024 x 1	14 x 14	100	PtSi	0.23	1986	NEC	59
64 x 128 IT	130 x 65	19	PtSi	0.26	1986	Valvo	26, 36
512 x 512 CSD	26 x 20	39	PtSi	0.22	1987	Mitsubishi	23
256 x 256 Hybrid	30 x 30	85	PtSi	0.23	1987	Hughes	40
256 x 1 MOS	60 x 25 to 60 x 200	57	PtSi	0.23	1987	Reticon	25
128 x 128 CTD-MOS (1T)	60 x 60	42	PtSi	0.23	1987	Reticon	24
4096 x 4	10 x 10	100	PtSi	0.22	1987	Mitsubishi	27
320 x 244 IT	40 x 40	43	PtSi	0.22	1988	Sarnoff	39
512 x 512 CSD	26 x 20	39	IrSi	0.17	1988	Mitsubishi	35
324 x 487 IT	42 x 21	42	PtSi	0.23	1988	NEC	49
190 x 244 IT	60 x 36	20	PtSi	0.205	1988	Loral Fairchild	50
320 x 244 IT	40 x 40	44	PtSi	0.22	1989	Sarnoff	48
256 x 244 IT	31 x 25	36	PtSi	0.22	1989	Loral Fairchild	51
512 x 244 IT	31 x 25	36	PtSi	0.22	1989	Loral Fairchild	51
512 x 512 LACA	30 x 30	54	PtSi	0.23	1989	Reticon	55
128 x 128 IT	29 x 48	52	IrSi	0.132	1989	MIT Lincoln Lab/Ford	45
640 x 486 IT 2ø not interlaced	25 x 25	54	PtSi	0.22	1990	Kodak	52
2048 x 16-TDI	30 x 30	43	PtSi	0.22	1990	Kodak	53
256 x 256 IT-CCD Meander-Channel, Al field plate not interlaced	40 x 40	52	PtSi	0.22	1990	Ford	58
400 x 244 Hybrid	24 x 24	84	PtSi	0.23	1990	Hughes	54
640 x 480 MOS (2T)	24 x 24	38	PtSi	0.22	1990	Sarnoff	63
128 x 128 DSI	50 x 50	100	PtSi	0.21	1990	Sarnoff	64

with PtSi SBDs for thermal imaging in the MWIR band and required active cooling at a temperature of about 80K[2] . A 4096 x 4-element multispectral linear array for remote-sensing applications in SWIR bands also used PtSi SBDs [27]. IrSi SBDs have been developed for extending the responsibility of SBD FPAs into the longwave infrared (LWIR) corresponding to the 8 to 10 μm band [28-30, 42, 44, 45].

2.0 SCHOTTKY-BARRIER DETECTORS

The first Schottky-barrier FPAs were made with thick Pd_2Si or PtSi detectors using about 600 Å of deposited palladium or platinum [2 - 5]. These FPAs exhibited relatively small photoresponse. More than an order of magnitude improvement in photoresponse was demonstrated in 1979 with 50 x 50-element FPAs constructed with thin PtSi SBDs at the David Sarnoff Research Center [6, 7]. The SBDs in this FPA had an optical cavity in the form of a thin (< 100 Å) PtSi layer separated from an aluminum reflector by a layer of deposited SiO_2. The general concept of a thin SBD with optical cavity was described in 1973 by Archer and Cohen for SBDs in the form of Au on p-type Si [69]. The improved PtSi SBD structure [6, 7, 9] resulted from a cooperative effort between the David Sarnoff Research Center[3] and the RADC, Hanscom AFB, MA. From 1980 to 1985, the fabrication process for the PtSi SBDs was optimized at Sarnoff with the development of 32 x 63, 64 x 128, and 160 x 244 IR-CCD FPAs [9, 10, 12, 16, 21]. Similar PtSi SBDs characteristics were also reported by Mitsubishi Corporation [8, 14, 18, 23], Fujitsu [15], NEC [59], and more recently by EG&G Reticon [24, 25, 55], Hughes [37, 54], Loral Fairchild [50, 51], Kodak [52, 53], and Ford Aerospace [58].

21 Operation of Schottky-Barrier Detectors

The basic construction and operation of a back-illuminated PtSi Schottky-barrier infrared detector integrated with a silicon CCD readout is illustrated in Fig. 1. The infrared radiation with photon energy less than the bandgap of silicon (Eg = 1.1 eV) is transmitted through the substrate. The absorption of the infrared radiation in the silicide layer results in the excitation of photocurrent across the Schottky-barrier (Ψ_{ms}) by internal photoemission. The "hot" holes (those that have sufficient energy to go over the Schottky barrier Ψ_{ms} formed between the silicide and the p-type silicon) are injected into the silicon substrate. Hence, a net negative charge will accumulate on the silicide electrode. Finally, the detection of the infrared optical signal is completed by transferring the negative charge from the silicide electrode into a CCD readout structure. This transfer is carried out either by a periodic voltage-reset readout or by a continuous (charge-skimming over the transfer barrier) readout [4]. The spectral energy window of a back-illuminated Schottky-barrier detector is

$$\Psi_{ms} < h\nu < Eg \qquad (1)$$

where

Ψ_{ms} is the metal-semiconductor Schottky barrier,
$h\nu$ is the photon energy, and
Eg is the silicon bandgap energy (1.1 eV).

22 Optimized Structure for PtSi SBD

To achieve maximum responsivity in the MWIR band, the PtSi SBDs are constructed with an "optical cavity" illustrated in Fig. 2 [13, 16]. The IR signal is introduced from the bottom side of the silicon substrate. About 20-Å-thick PtSi film is formed on p-type silicon substrate and is separated from an aluminum reflector by about a quarter-wave-thick SiO or SiO_2 dielectric layer. This maximizes the

---

2 With the exception of the 4096 x 4 scanning FPA [27] all PtSi FPAs illustrated in Table 1 were developed for thermal imaging in the MWIR band.

3 Formerly RCA Laboratories.

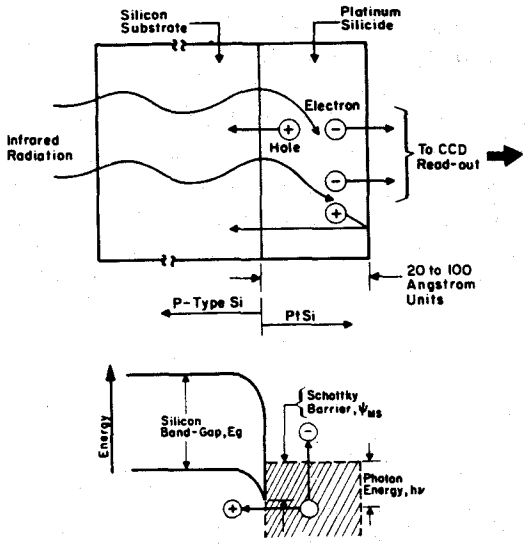

Fig. 1. Operation of Schottky-barrier detector.

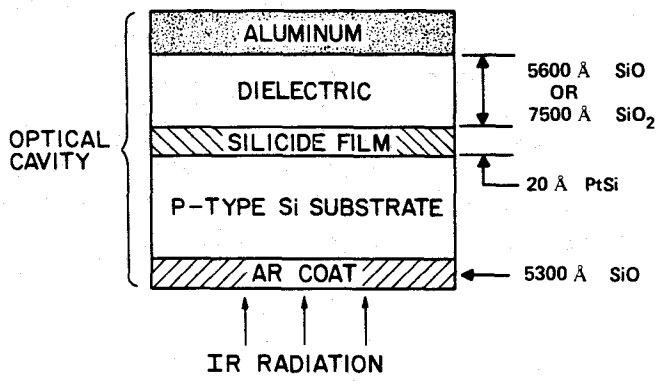

Fig. 2. Cross-sectional view of PtSi SBD with optical cavity tuned for maximum response at a wavelength of 4.3 μm.

optical absorptance by setting up a peak of an optical standing wave at the thin PtSi film[4]. An antireflective (AR) coat, deposited on the back side of the silicon substrate, increases the coupling of the IR radiation into the SBD by about 30 percent.

The responsivity, R, of the Schottky-barrier detector can be approximated by a Fowler equation [70] as

$$R = C_1 \left(1 - \frac{\Psi_{ms}\,\lambda}{1.24}\right)^2$$

where

- R is the responsivity in A/W,
- C_1 is the quantum efficiency coefficient in eV^{-1}
- Ψ_{ms} is the metal-semiconductor Schottky barrier in eV, and
- λ is the wavelength of the infrared radiation.

According to the photoemission model developed by Cohen et al [70] for electron emission in the case of a SBD with infinitely thick metal, the C_1 coefficient can be expressed as:

$$C_1 = \frac{1}{8\,[E_f + \Psi_{ms}]} \qquad (3)$$

However, according to the model derived for hole emission the C_1 coefficients for a very thin PtSi SBD on a p-type silicon substrate can be expressed [13, 16, 21] as

$$C_1 = \frac{A(\lambda)\,G(\lambda)}{8\,\Psi_{ms}} \qquad (4)$$

where

- $A(\lambda)$ is the optical absorptance in the PtSi film and
- $G(\lambda)$ is the internal injection efficiency gain (as compared to the thick-film silicide) of hot holes due to multiple reflections at the boundaries of thin film of PtSi.

---

4 IR signal has been introduced on the silicide-side of the SBD to achieve a broad spectral response including infrared, visible, and ultraviolet [46] and in the case of direct Schottky injection for achieving 100% fill factor [65].

At this point, it should also be pointed out that value of C_1 coefficient computed by Eq. (4) was found to be consistent with experiment for thin PtSi SBDs in predicting the optimum thickness of about 20Å for the PtSi layer for the case of thermal imaging in the MWIR band [13, 16, 21]. On the other hand Eq. (3) derived for electron emission appears to predict low values for the C_1 coefficient of PtSi SBDs [34].

The original data on the effect of the thickness t of the PtSi film on SBD photo-yield parameters at 4.0 μm is illustrated in Fig. 3. This figure shows the curves of (a) absorptance A of PtSi, (b) internal injection efficiency gain G and (c) product AG as a function of PtSi layer thickness normalized to the absorption length estimated to be 200 Å. The curve for the absorptance A - computed using Fresnel equations for a PtSi film on a silicon substrate - is compared with measured experimental points (triangles) at the wavelength $\lambda = 4.0$ μm [13, 21].

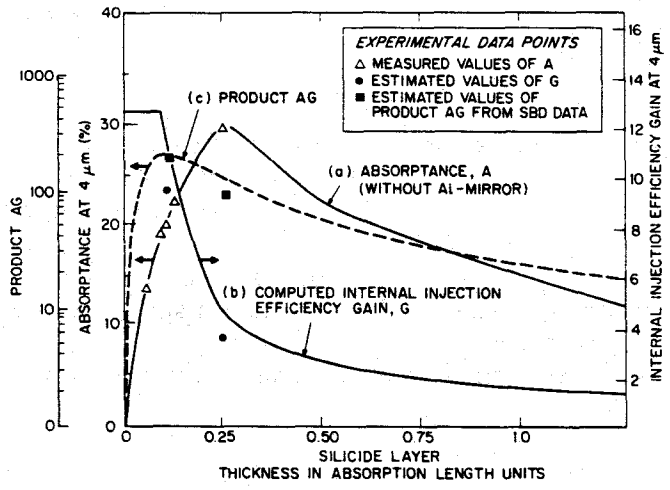

Fig. 3. Optimization of PtSi SBD photoyield at 4.0 μm as a function of the silicide thickness.

2.3 Responsivity and Dark Current Characteristics

Responsivity data for PtSi and Pd_2Si SBDs reported by the David Sarnoff Research Center is shown in Fig. 4 [12, 13, 16, 21]. Also shown in this figure are responsivities of SBDs of mixed silicides (Pt, Ni)Si and (Pt, Pd)Si. Inspection of Fig. 4 shows that PtSi SBD can be made with the Schottky barrier, Ψ_{ms}, in the range of 0.190 to 0.218 eV by controlling the thickness of the deposited Pt and the anneal time [21]. Thinner films of PtSi with shorter anneals result in SBDs with a higher responsivity as well as a higher dark current characterized by a Schottky barrier, Ψ_{ms}, in the range of 0.19 to 0.20 eV [21].

A study of the responsivity/dark-current tradeoff showed that the use of a thicker PtSi together with a long anneal time produces SBDs with lowest dark current, obtained with some sacrifice of responsivity [21]. Typical responsivities obtained for Pd_2Si SBDs designed for passive-cooling operation at a temperature of 120K in the SWIR band [12, 22] and PtSi SBD designed for thermal imaging in the MWIR band at a temperature in the range of 77 to 80K [21] are shown in Fig. 4. Although higher responsivities were previously reported for PtSi test SBDs [21], the present state-of-the-art for high-performance PtSi SBDs for thermal imaging can be represented by the responsivity shown in Fig. 5 [31, 48].

In fact, the responsivity of PtSi SBDs measured directly on the focal plane arrays is usually found to be even somewhat lower because the quoted fill factors [21] usually are based on nominal mask dimensions and normally do not include the reduction of active detector area due to the n-type SBD guard rings.

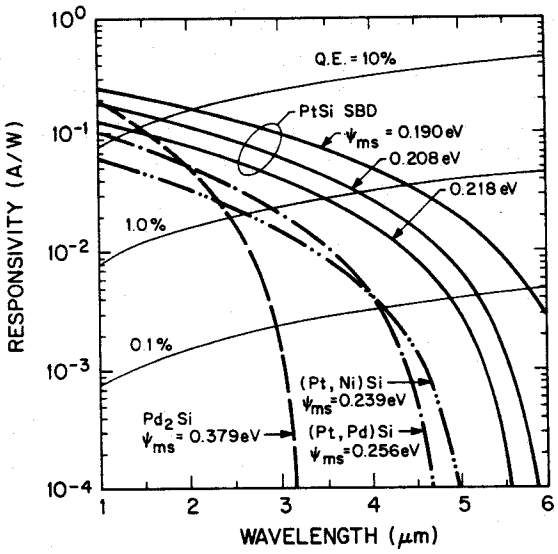

Fig. 4. Responsivities of PtSi (Pt, Si)Si, (Pt, Pd)Si and Pd_2Si Schottky-Barrier detectors.

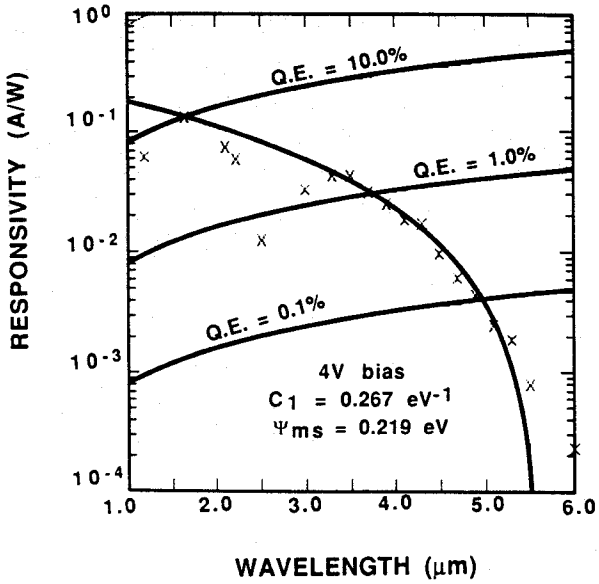

Fig. 5. Measured responsivity at 4V bias for PtSi SBD with $C_1 = 0.267\ eV^{-1}$ and Ψ_{ms} 0.219 eV.

The dark current of SBDs is a strong function of processing conditions and substrate doping. The dark current density representative of the best quality PtSi SBDs is shown in Fig. 6 for temperature of 77 and 87K and as a function of SBD bias voltage.

According to the thermionic emission model [71] the reverse-bias saturation current density, J_D, in A/cm^2 can be expressed as:

$$J_D = A^* T^2 e^{-q\Psi_{ms}/kT} \qquad (5)$$

where

- A^* is the Richardson emission constant for holes in silicon (ideally 32 A/cm^2K^2),
- T is the detector temperature in K,
- q is the electronic charge in Coulomb,
- Ψ_{ms} is the activation energy or the Schottky barrier in eV, and
- k is the Boltzmann constant.

The dark current measurements for PtSi SBDs show that the dark current increases exponentially with temperature with an activation energy that is equal or lower than the Schottky-barrier potential Ψ_{ms} obtained by the photoemission measurements [16, 21]. Therefore, for some applications it may be desirable to use SBDs with a Schottky barrier in the range between PtSi and Pd_2Si (i.e. 0.24 - 0.26 eV) that can be obtained with mixed silicides such as shown in Fig. 4. Finally, for applications in the 1-2 μm range NiSi with Ψ_{ms} of 0.48 eV offers the possibility of dark current of less than 1.0 nA/cm^2 for operation at a temperature in the range of 150 - 160K [47].

According to Eq. (2), the cut-off wavelength, λ_c, can be expressed as:

$$\lambda_c = \frac{1.24}{\Psi_{ms}} . \qquad (6)$$

For typical PtSi SBDs with Ψ_{ms} of 0.22 eV the value of λ_c is 5.7 μm. The cut-off wavelength can be extended with electric-field-induced barrier lowering obtained by increasing the substrate doping for the SBDs using a shallow implant [32, 33]. However, the most successful approach for extending the long wave response to λ_c of has been achieved by IrSi SBDs [44, 45]. A barrier height of 0.152 eV corresponding to a cut-off wavelength of 8.2 μm and measured by internal photoemission was reported by Pellegrini et al [28, 29] for an IrSi SBD with C_1 of 0.051 eV^{-1} and Ψ_{ms} of 0.155 eV obtained from dark current measurements. A cut-off wavelength of 9.2 μm corresponding to Ψ_{ms} of 0.135 eV and C_1 coefficient of 0.075 eV^{-1} were reported by Tsaur, Weeks, and Pellegrini for Pt-Ir silicide SBDs [42]. These SBDs were formed by deposition 5Å of Pt followed by a second deposition of 15Å of Ir. The longest cut-off wavelength of 10 μm corresponding to Ψ_{ms} of 0.122 eV was reported by Tsaur et al [44]. The responsivity of this IrSi SBD with a comparison to a PtSi SBD is illustrated in Fig. 7.

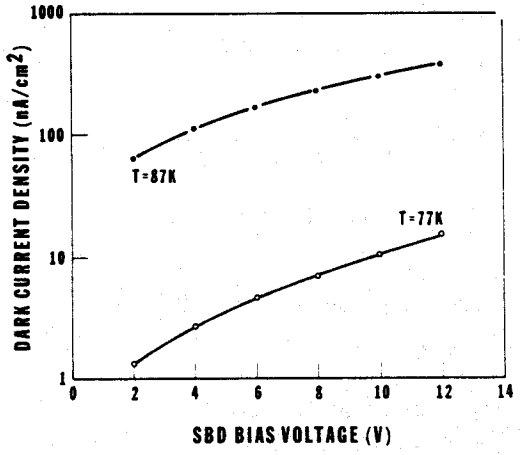

Fig. 6. Dark current density vs bias voltage for PtSi SBD of Fig. 5.

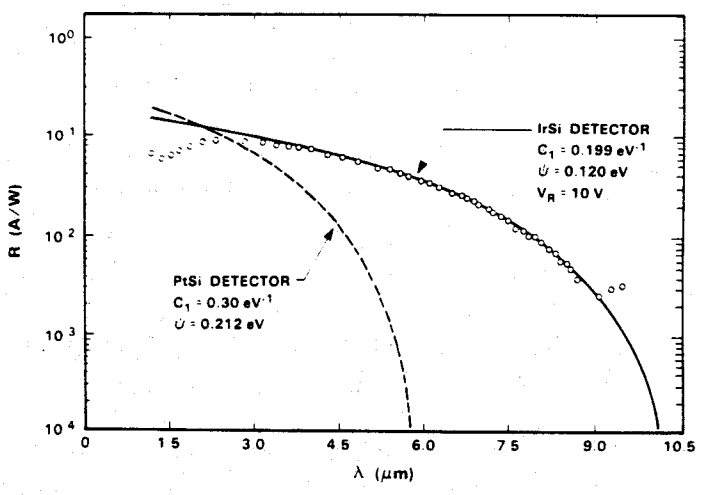

Fig. 7. Responsivities of IrSi and PtSi SBDs (Tsaur - 1988).

A 512 x 512 charge sweep device (CSD) image sensor with IrSi SBDs was reported by Yutani et al [30]. In this case, IrSi SBDs were characterized by C_1 of 0.035 eV^{-1} and Ψ_{ms} obtained by internal photoemission of 0.17 eV corresponding to λ_c of 7.3 μm and Ψ_{ms} calculated from dark current characteristics of 0.156 eV. To reduce the dark current to the value of PtSi SBD operating at 82K, the IrSi SBDs were operated at 62K, representing the minimum operating temperature at which the transfer losses of the horizontal CCD did not degrade the resolution of the imager. Thermal imaging with a 7.2-μm long-pass filter achieving a noise equivalent temperature of 0.3K was demonstrated by Tsaur, McNutt, Bredthauer, and Mattson with a 128 x 128 element surface-channel IT-CCD array [45]. This array was operated at 50K and the cut-off wavelength of the IrSi SBDs was 9.4 μm.

24 SBD Fabrication

The main advantage of the SBD FPAs is that they can be fabricated as monolithic arrays in a standard silicon VLSI process. Typically, the silicon array is completed up to the Al metalizatial step. At this point a Schottky-contact mask is used to open SiO_2 surfaces to silicon at the SBD locations. In the case of PtSi SBDs, a very thin layer of Pt (10 to 20 Å) is deposited and sintered (annealed) to form PtSi and the unreacted Pt on the SiO_2 surfaces is removed by dip-etching in hot aqua regia [21]. The SBD structure is then completed by a deposition of a suitable dielectric (such as SiO_2) for forming the SBD "resonant cavity", removing this dielectric outside the SBD regions, and depositing and defining Al for the SBD reflector and the interconnects of the Si readout multiplexer.

In the case of the 10-μm IrSi SBDs, the IrSi was formed by in-situ vacuum annealing and the unreacted Ir was removed by reactive ion etching [44]. The quality of the resulting IrSi film is illustrated in Fig. 8.

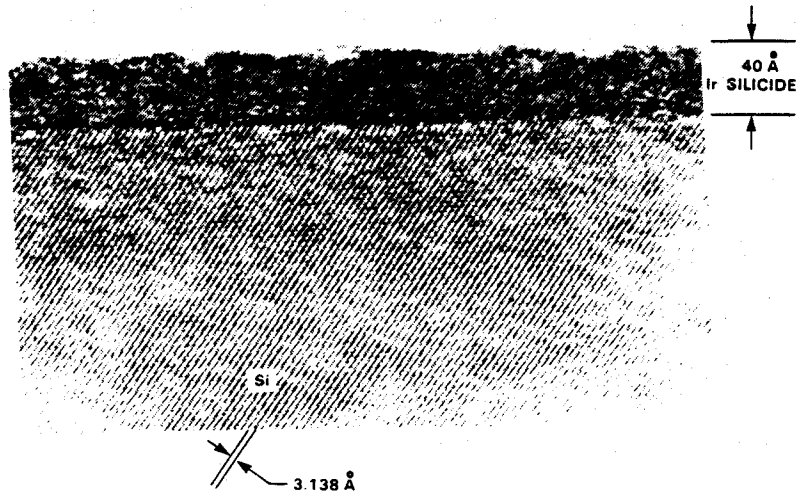

Fig. 8. High-resolution cross-sectional TEM image of IrSi sample prepared by in-situ vacuum annealing (Tsaur - 1988).

3.0 REPORTED SBD IMAGE SENSORS

The general characteristics of the reported FPAs are summarized in Table 1. This table compares the number of elements and CCD designs, pixel sizes, fill factors (defined as the ratio of the active SBD area to the pixel area), types of SBDs characterized by a Schottky barrier, Ψ_{ms}, the year when each FPA was first reported, by which company, and where referenced. Most of the monolithic area sensing SBD FPAs were constructed as interline transfer (IT) imagers [4, 7 - 9, 11, 13 - 16, 26, 31, 36, 39, 45, 48-52, 58]. The SBD FPAs developed at Valvo represent the only reported IT-CCD imagers with a charge skimming structure that could be used for exposure control or background subtruction [26, 39]. The only two noninterlaced IT-CCD FPAs are the 640 x 480 FPA reported by Kodak [52] and the 256 x 256 FPA reported by Ford Aerospace [58]. SBD FPAs with MOS readout MOS (1T) with one MOSFET per SBD and MOS (2T) with two MOSFETs per SBD were developed to improve the trade-off between the fill factor and charge handling capacity [18, 63]. An 85% fill factor was achieved by Hughes with a 256 x 256 400 x 256 hybrid FPAs with a form of MOS readout with on-chip switched integrators [40, 54]. The 512 x 512-element charge-sweep device (CSD) developed by Mitsubishi Corporation allows an output multiplexer with large charge handling capacity and a low-noise CCD readout [23, 35].

4.0 SCANNING FPAs

Inspection of Table 1 shows the progress in the development of the SBD scanning (line sensing) FPAs. The first line sensor in the form of a 256 x 1 PtSi IR-CCD FPA was designed for operation either in a conventional detector reset mode or a "continuous charge skimming" mode [4]. A buttable dual band 512 x 2 IR-CCD FPA with Pd_2Si SBD was developed for spaceborne remote sensing in the SWIR band and for operation with passive cooling [22]. This line sensor had 30-μm x 30-μm pixels with a fill factor of 70-87% depending on the construction of the SBD guard rings [76]. A family of 256-element PtSi-SBD line sensors with MOS readout was announced by EG&G Reticon for Spectroscopic applications [24]. These line

sensors area available with a fill factor of 57% and a choice of pixel format corresponding to 60 (H)-μm x 25 (V)-μm, 60 (H)-μm x 50 (V)-μm, 60 (H)-μm x 100 (V)-μm, and 60 (H)-μm x 200 (V)-μm. A 100% fill factor was achieved for the 1024 x 1 FPA with a bilinear CCD readout and 14-μm x 14-μm staggered SBDs developed by NEC [59] and for the 4096 x 4 FPA with four bands of bilinear CCD line sensors with 10-μm x 10-μm staggered SBDs developed by Mitsubishi Corporation for remote sensing space applications [27, 38]. The most recently reported SBD scanning FPA is the 2048 x 16 TDI PtSi IR imaging CCD array developed jointly by Itek and Kodak [53]. This TDI-CCD array has 30-μm x 30-μm pixels with 43% fill factor has been constructed in the form of 2-phase CCDs with four parallel 512 x 16 sections per chip to be buttable into higher resolution arrays for remote sensing applications.

5.0 STARING FPAs

5.1 Design Trade-Offs

The design of a staring (area sensing) FPA with SBDs involves a trade-off of the following parameters and considerations:

- Resolution
  - number of pixels
  - pixel size
  - chip size
- Charge Handling Capacity
  - Q_{max} in electrons/pixel
- Fill Factor
  - SBD responsivity
  - MTF
- Available FPA Designs
  - Interline Transfer (IT-CCD)
    - interlaced : Sarnoff [21, 48], NEC [49], Fairchild [51]
    - uninterlaced : Kodak [52], Ford [58]
  - Charge Sweep Device (CSD)
    - Mitsubishi [23]
  - Line Addressed-Accumulation Readout (LACA)
    - EG&G Reticon [55]
  - SBD Readout by MOS Switches
    - One MOSFET per SBD (MOS 1T) : Mitsubishi [18], Reticon [24]
    - Two MOSFET per SBD (MOS 2T) : Sarnoff [63]
  - Hybrid FPA with switched integrating amplifiers (Hybrid)
    - Hughes [40, 54]
  - Direct Schottky Injection [DSI]
    - Monolithic FPA with 100% fill factor : Sarnoff [64]

The interplay of the above considerations and the expected performance in the terms of the noise equivalent temperature of the staring FPAs will be reviewed in the following sections.

5.2 Noise Equivalent Temperature

The noise equivalent temperautre, NEΔT, representing the total output temporal (or pixel) noise at a given background temperature converted into an equivalent temperature difference at the background scene, is a very effective figure of merit for a staring FPA. The noise equivalent temperature for an FPA is normally measured as:

$$NE\Delta T = \frac{N_{noise}}{\Delta N_B/\Delta T} \text{ (K)} \qquad (7)$$

where

N_{noise} is the measured temporal pixel noise in rms electrons/pixel and

$\Delta N_B/\Delta T$ is the measured FPA responsivity in electrons/pixel/K for a background signal N_B in electrons/pixel.

For thermal imaging operation of the SBD FPAs with background (shot noise) limited performance (BLIP), that can be achieved with PtSi FPAs [21, 48, 67], the noise equivalent temperature can be expressed as:

$$NE\Delta T = \frac{\sqrt{N_B}}{C\,N_B} = \frac{1}{C\sqrt{N_B}} \tag{8}$$

where

C is contrasted ($\Delta N_B/N_B/\Delta T$) and

N_B is the detected signal as a given background temperature in electrons/pixel

Assuming a highly efficient FPA cold shield the volume of contrast for 300K background for radiation in the 3 to 4.3 μm band can be estimated as C = 0.035/K. The data reproted for the Sarnoff 320 x 244 FPA operating at 30 frames/s with f/1.4 optics gives $\Delta N_B/\Delta T$ of 2.1 x 10^4 electrons/K for N_B of 5 x 10^5 electrons/pixels [39, 48]. The resulting value of C is 0.042/K. The above value of measure contrast could be compared with the data for the Kodak 640 x 486 FPA operating at 30 frames/s with f/2.8 cold stop for which $\Delta N_B/\Delta T$ is reported as 3,200 electrons/pixel for N_B of 100,000 electrons/pixel [51]. For the second case the measured value of contrast can be estimated as C = 0.032/K.

To illustrate the requirement of the charge handling capacity (Q_{max}) on the thermal imaging performance of the staring FPA, Table 3 shows the calculated values of the noise equivalent temperature, ($NE\Delta T$) for contrast (C) of 0.02/K and 0.04/K as function of the detected background signal (N_B) assuming a background (shot noise) limited performance (BLIP).

Table 2. Calculated $NE\Delta T$ for Background (Shot Noise) Limited Performance (BLIP) of Staring FPAs.

N_B (electrons/pixel)	$NE\Delta T$ (K)	
	C = 0.02/K	C = 0.04/K
10^5	0.16	0.08
2 x 10^5	0.11	0.056
5 x 10^5	0.07	0.035
10^6	0.05	0.0250

5.3 Interline Transfer CCD FPAs

The SBD FPA with an interline transfer CCD (IT-CCD) readout is illustrated in Fig. 9. The construction of this type of FPA involves a tradeoff between the fill factor of the imager and the charge handling capacity (Q_{max}) of the CCD readout multiplexer [21]. To improve both of the above parameters, these FPAs have been made with 2:1 vertical interlace [39, 48-51], thus, increasing Q_{max} by a factor of 2x over the non-interlace design. Non-interlaced (progressive scan) IT-CCD FPAs [14, 52, 58], however, have the advantage of less flicker and are more suitable for machine vision and tracking operations. The data shows that for SBDs formed on 30 to 50 ohm-cm p-type Si substrates and buried-channel CCD (BCCD) registers formed by a phosphorus implant with a dose of 1.3 x $10^{12}cm^{-2}$, the maximum charge

density of the BCCD register (depending on operating conditions) is from 3500 to 6000 electrons/μm^2 and the area of a half stage of the BCCD register must be equal or greater than 1/5 of the total detector area including the n-type guard rings [21].

5.3.1 Sarnoff 320 x 244 IT-CCD

A 320 x 244-element IT-IR-CCD with 40-μm x 40-μm pixels was developed by David Sarnoff Research Center with the support of Rome Air Development Center, Hanscom AFB, MA. This FPA was fabricated with 2-μm minimum design rules using a self aligning process [39, 40, 48]. It has a fill factor of 43% and charge handling capacity of 1.4×10^6 electrons/pixel. To maximize the charge handling capacity this imager was designed for operation with 4-phase two-level-polysilicon CCD readout. The layout and the cross-section of the pixel for this FPA are shown in Figs. 10 and 11(a). It should be noted that in this design the RC time constant of the vertical CCD clock is reduced by strapping every forth vertical CCD gate with a vertical aluminum buss. Figures 11(b) and Fig. 12 illustrate the charge readout from the SBD to a buried-channel CCD register. To minimize dark-current spikes, the PtSi SBD's are surrounded by n-type guard rings, self-aligned to the polysilicon gates. The channel stops between two adjacent SBD's in the vertical direction and the SBD's and buried-channel CCD (BCCD) readout registers are in the form of p-type and surface-channel CCD (SCCD) regions, respectively.

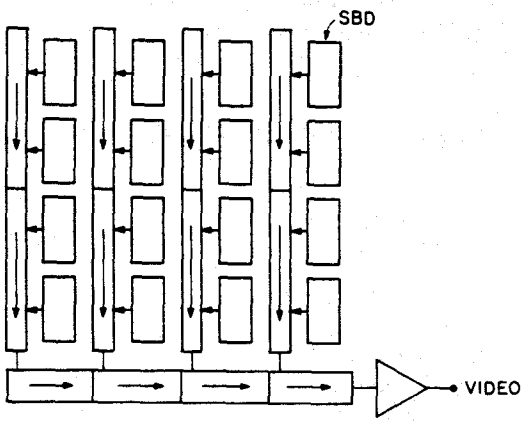

Fig. 9. SBD FPA with vertically interlaced IT-CCD readout.

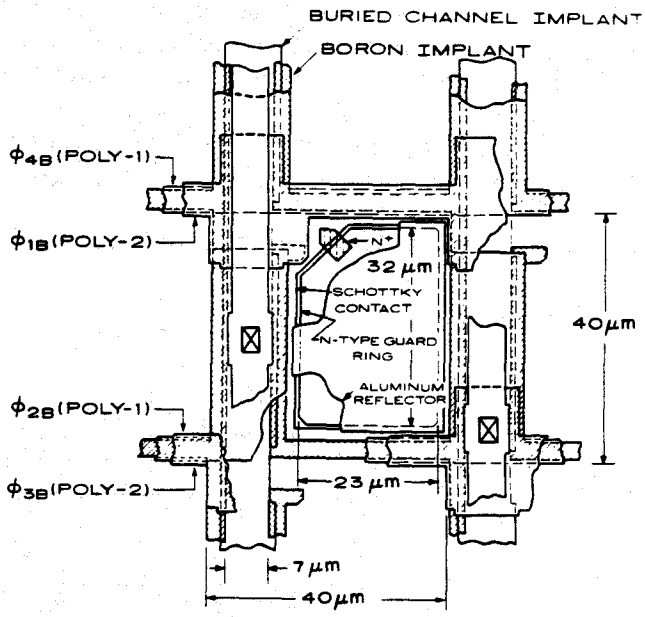

Fig. 10. Pixel layout of the 320 x 244 FPA.

As illustrated by the channel potentials in Fig. 12, the SCCD channel stops are driven into accumulation by the clock pulses ($\Delta\phi_B$) during the CCD-charge-transfer operation of the parallel CCD register. At the end of the optical integration time (T_i), the CCD transfer gate is driven to a positive potential V_{BT}, as illustrated in Figs. 11(b) and 12. This operation resets the SBD electrode to reference Potential 2 (Fig. 12(b)) corresponding to $\Psi_{T\text{-}SCCD}$ (Fig. 12) and transfers the detected charge signal Q_D into the CCD well. During this charge transfer, a higher barrier potential is formed under the implanted p-type channel stop on the left side of the SBD to provide directionality of the signal-charge flow during the SBD charge readout.

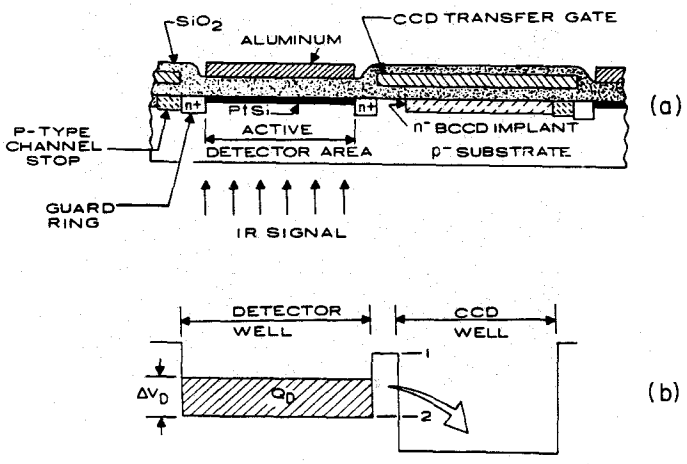

Fig. 11. Construction and operation of SBD with BCCD readout.

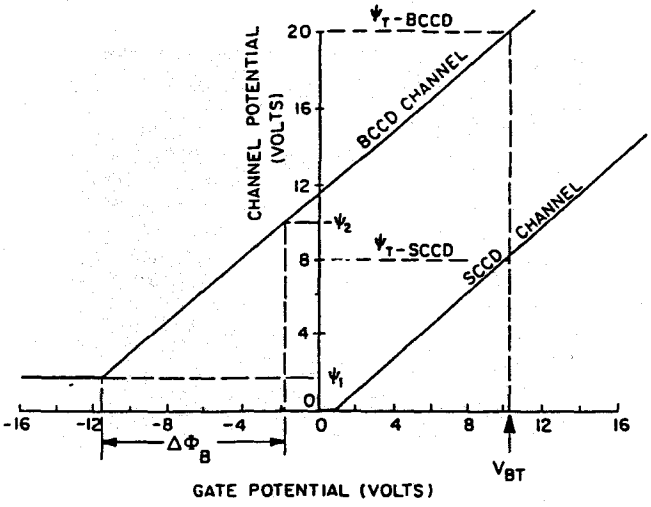

Fig. 12. Curves of the channel potential vs. gate voltage for a buried-channel CCD and a surface-channel CCD illustrating the operation of the SBD readout.

The operation of the SCCD channel-stop regions into accumulation assures an operational blooming control mode of the SBD's, provided the BCCD readout register has a sufficient charge-handling capacity [4, 21].

The infrared imaging performance of the 320 x 244 FPA with one-point uniformity corrector for operation at 30 frames/s with 3.4-μm long-pass filter and f/1.4 optics is illustrated in Fig. 13(a) showing a thermal imaging of man's face and in Fig. 13(b) a thermal image of a 0.1K test pattern. Excellent uncorrected imaging obtained with a 320 x 244 FPA is illustrated in Fig. 14. A shot-noise limited performance of the 320 x 244 FPA is illustrated in Fig. 15. It should also be added that Mooney showed that no 1/f noise is observable with the PtSi SBD FPAs [68].

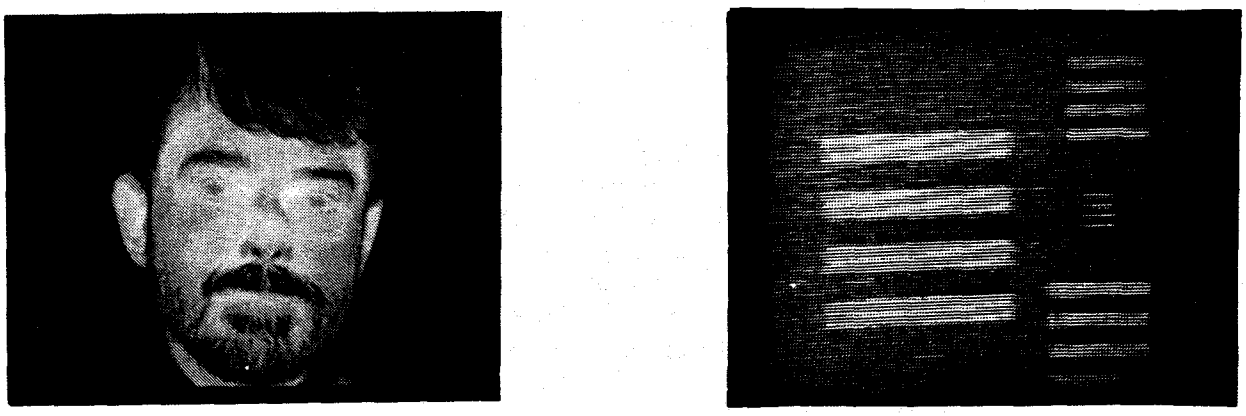

(a) (b)

Fig. 13. Thermal imaging obtained 320 x 244 FPA operating with one-point uniformity corrector, 30 frames/s and f/1.4 optics showing a man's face in (a) and a 0.1K test pattern in (b).

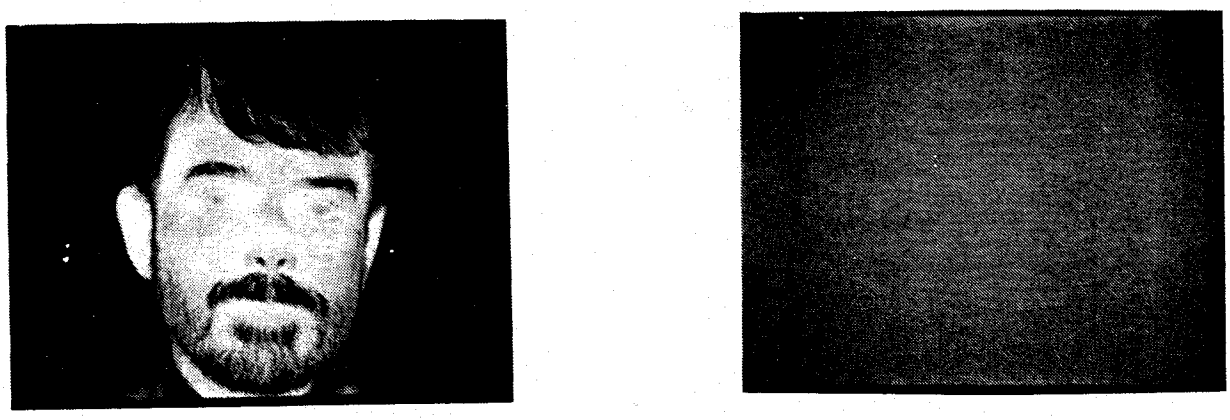

(a) (b)

Fig. 14. Uncorrected thermal imaging with a very uniform 320 x 244 FPA showing a man's face in (a) and a 300K background in (b).

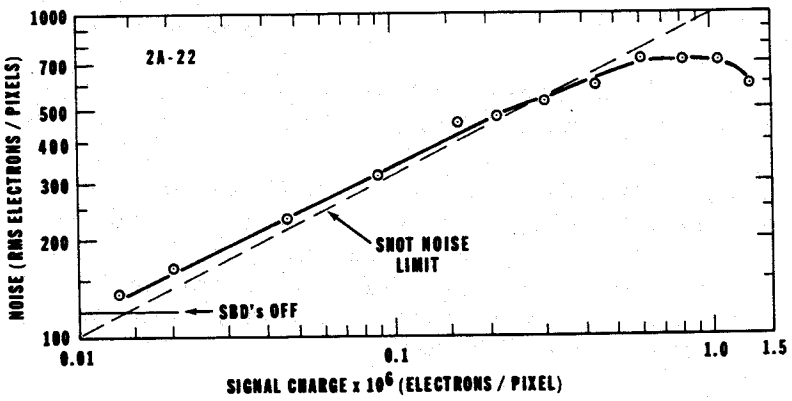

Fig. 15. Measured readout noise vs. charge signal for 320 x 244 FPA.

5.3.2 NEC 324 x 487 IT-CCD FPA

A 324 x 487-element interlaced IT-CCD FPA with 42 (H)-μm x 21 (V)-μm pixels and 42% fill factor was developed by NEC [49]. This imager was constructed with 1.5-μm design rules in the form of a two-level polysilicon and two-level metal structure. The unique feature of this FPA is a gate control drain structure of the vertical CCD registers which allows electronic shutter operation and expansion of the dynamic range by a "knee characteristic" that represents an effective gamma control function. The 324 x 487 FPA achieving NEΔT of 0.1K for operation at 30 frames/s and f/1.0 optics [49]. The maximum signal (Q_{max}) of this FPA was not reported but is estimated to be in the range of 2 to 3 x 10^5 electrons/pixel.

5.3.3 Fairchild 512 x 488 IT-CCD FPA

A non-interlaced 512 x 488-element IT-CCD FPA with 31.5 (H)-μm x 25 (V)-μm pixels and 36% fill factor was developed by Loral Fairchild [51]. This FPA has been constructed with 1.8-μm design rules, Q_{max} of 5.5 x 10^5 electrons/pixel, and is capable of NEΔT of 0.07K with f/1.8 optics [51]. Thermal imaging reported by Loral Fairchild is shown in Fig. 16.

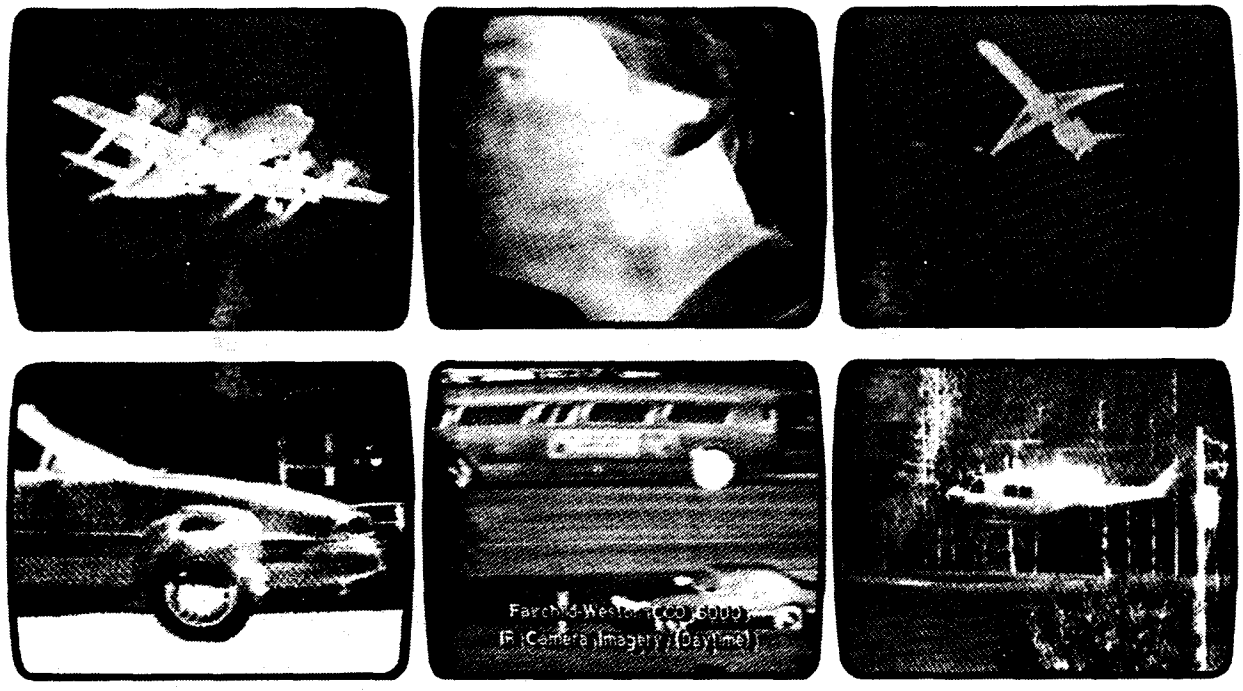

Fig. 16. Thermal imaging obtained with Fairchild 512 x 488 FPA.

5.3.4 Kodak 640 x 486 IT-CCD FPA

A non-interlaced 640 x 486 IT-CCD FPA 25-μm x 25-μm pixels and 54% fill factor was developed by Kodak [52]. This FPA was constructed using a 2-phase two-level polysilicon buried-channel CCD process [72] and 1.2-μm design rules. This FPA has Q_{max} of 2.2 x 10^5 electrons/pixel and reported to have NEΔT of 0.15K for operation with f/2.8 cold shield. The design and layout of the Kodak 640 x 486 non-interlaced IT-CCD FPA in the form four parallel 160 x 486 sections is illustrated by Figs. 17(a) and (b). The pixel layout for this FPA is shown in Fig. 17(c).

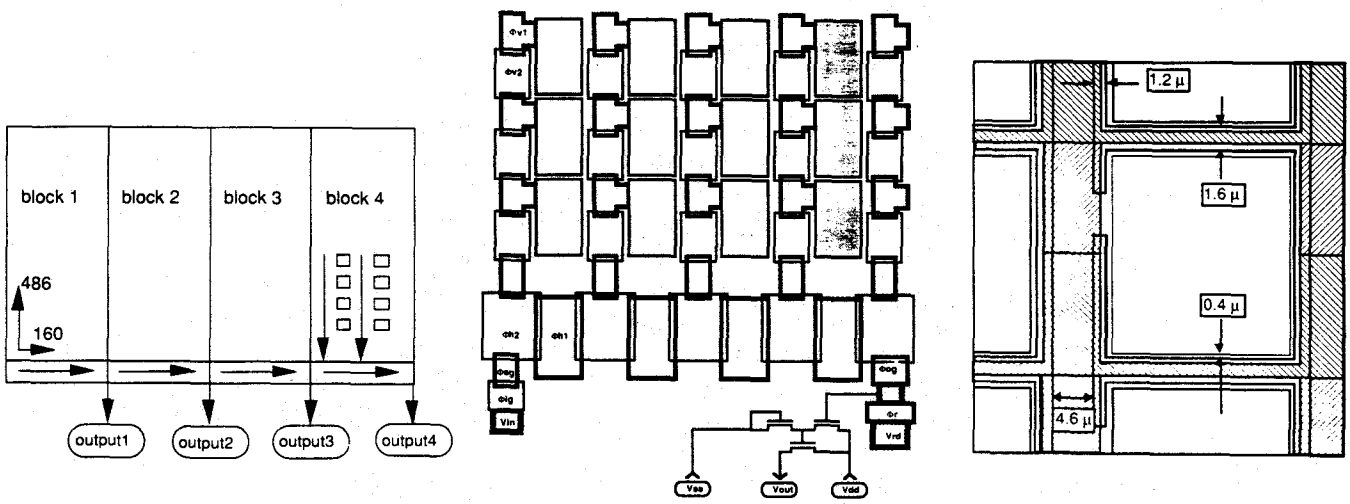

(a) (b) (c)

Fig. 17. Kodak 640 x 488 uninterlaced IT-CCD FPA showing a block diagram of the imager in (a), schematic of one quadrant in (b), and the pixel layout in (c).

5.3.5 Ford 256 x 256 IT-CCD FPA

A family of 128 x 128, 256 x 256, 256 x 244, and 640 x 488 high-fill-factor non-interlaced IT-CCD FPAs with 4-phase meander channel BCCD readout and aluminum-field-plate SBD guard rings was reported by Ford Aerospace Corporation [58]. The 256 x 256 FPA with 40-μm x 40-μm SBD and 52% fill factor for 3.0-μm design rules has Q_{max} of 1.2 x 10^6 electrons/pixel. This FPA for operation at 30 frames/s with f/2.4 lens was reported to have NEΔT of 0.1K. The combination of the aluminum-field-plate SBD guard [73] (illustrated in Fig. 18(b)) with a 4-phase meander-channel BCCD readout register (shown in Fig. 19) results in a large fill factor and a large charge handling capacity [58].

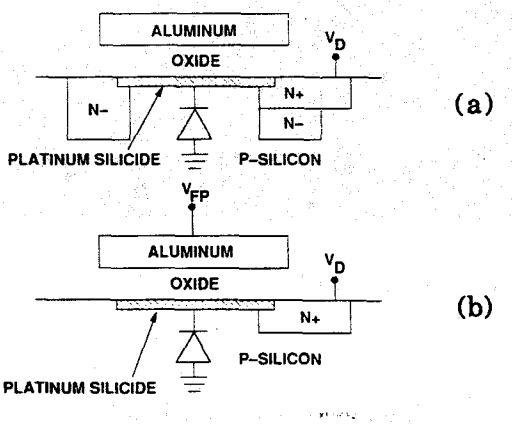

Fig. 18. Comparison of SBD construction with a standard N^- guarding ring in (a) and aluminum-field-plate guardring in (b).

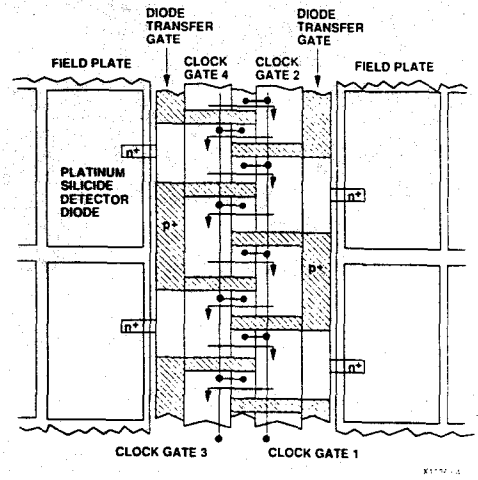

Fig. 19. Pixel layout of the Ford 256 x 256 FPA (McNutt-1990).

5.3.6 Mitsubishi 512 x 512 CSD FPA

A 512 x 512 Charge Sweep Device (CSD) SBD FPA developed by Mitsubishi Corporation is illustrated in Fig. 20 [23, 35]. The CSD imager consists of minimum-geometry parallel array of vertical CCD registers integrated with a high-fill-factor SBD array. During the operation of the CSD FPA, the detected charge signal (corresponding to two rows of SBDs combined into one horizontal line) is transferred to the minimum-geometry vertical registers under the control of the vertical scan switch. Then, during the readout of the previous horizontal line by the serial CCD output register, the transferred charge corresponding to one horizontal line is swept by the CSD clock into the parallel line-storage register. From there, during the horizontal blanking time, the content of the line storage register is transferred into the serial output register to be sequentially readout to as the output video. A comparison of the layout for 26 (H)-μm x 20 (V)-μm pixels for IR-CCD and CSD FPAs with 2-μm design rules is illustrated in Fig. 21.

The Mitsubishi 512 x 512 CSD FPA was constructed with 2-μm design rules and has 39% fill factor. This imager is operated in a field integration mode with a vertically interlaced readout of two SBDs per pixel. The Q_{max} of the CSD FPA is limited by SBD capacitance. For SBD reset voltage of 4V, Q_{max} of 7.5 x 10^5 electrons/pixel was reported [35] and Q_{max} of 1.4 x 10^6 electrons/pixel for SBD reset voltage of 11V [57]. The corresponding reported NEΔT values for this FPA are 0.1K for f/1.5 optics [35] and 0.07K for f/1.2 optics [57]. Examples of thermal imaging obtained with the 512 x 512 CSD IR camera are shown in Fig. 22.

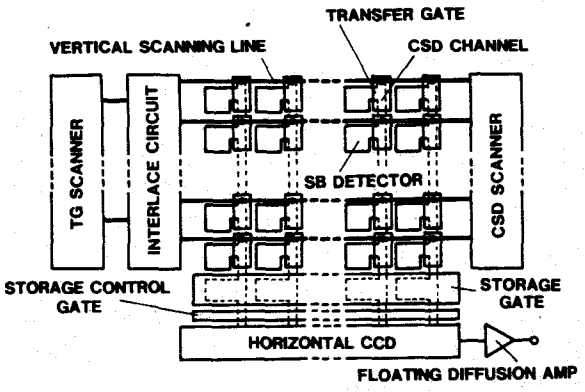

Fig. 20. Block diagram of 512 x 512 CSD imager with PtSi SBDs (Kimata-1987).

ITEM	IL-CCD	CSD
PIXEL LAYOUT	7μm	2μm
FILL FACTOR	30%	43%
RESPONSIVITY	1	1.43
SATURATION	1	1.33

PIXEL SIZE=26(H)x20(V)μm²

Fig. 21. Comparison of IT-CCD and CSD FPA pixel design (Kimata-1987).

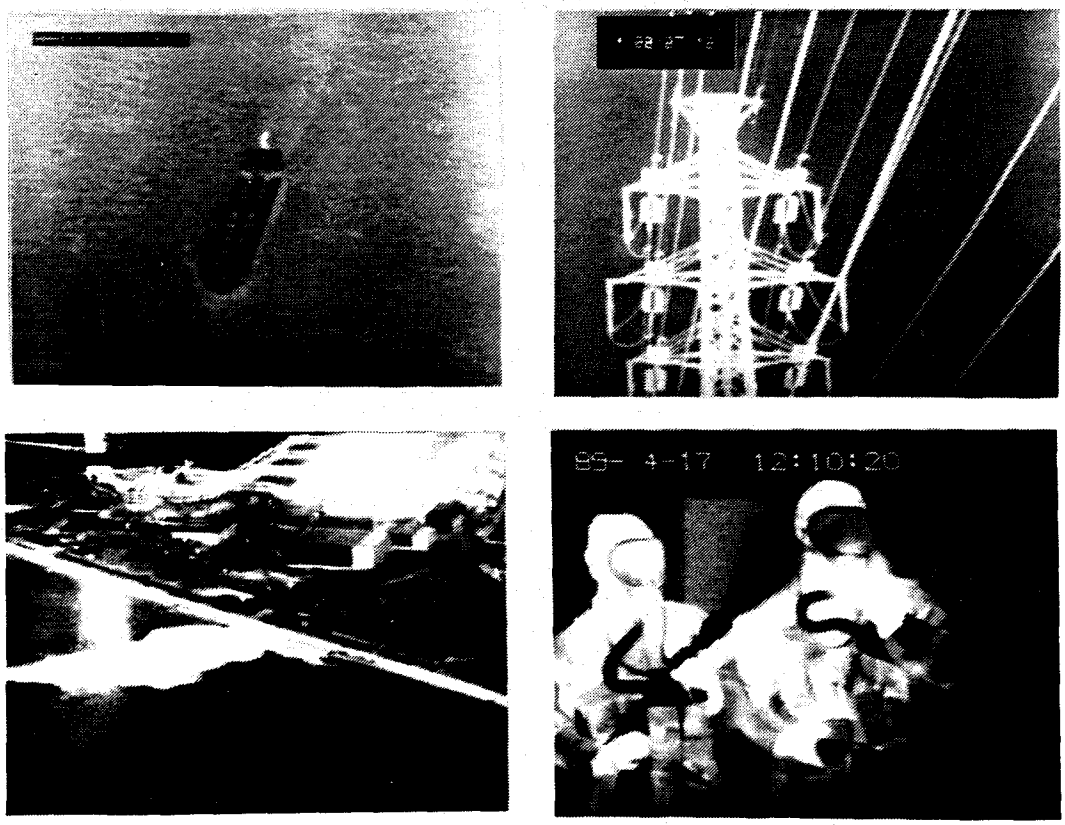

Fig. 22. Thermal image detected by the 512 x 512 CSD IR TV camera operating with f/1.5 optics (Mitsubishi-1989).

The advantages of the CSD SBD FPA are: large fill factor, large maximum signal charge that is only limited by the SBD capacitance and voltage, and low readout noise of the CCD output register. To avoid large power dissipation, the parallel charge-sweeping registers are operated at a rather low clock voltage of 1 to 2V.

5.3.7 LACA FPA

A 512 x 512-element FPA with a Line-Addressed Charge-Accumulation (LACA) readout structure was developed by EG&G Reticon [55]. This FPA has 30-μm x 30-μm pixels and 54% fill factor obtained with 2.0 μm process design rules. The construction and operation of the LACA FPA is similar to that of the CSD FPA. However, while in the case of the CSD imager, the detected signal is transferred out of the SBDs in the selected horizontal line once per line time followed by a charge sweep transfer by the minimum geometry vertical CCD register, the LACA imager operates with the transfer of charge from the selected line of SBDs synchronized to a multiple of clock cycles of the vertical CCD registers. Thus, the detected signal charge packets are separated by several empty stages of the vertical CCD register and the charge sweeping operation involving these empty stages can be used to improve the charge-transfer efficiency and/or to increase the charge handling capacity. The main advantage of a LACA FPA over a CSD FPAs is a lower power dissipation due to lower clock frequency of the vertical registers [55].

A block diagram of the 512 x 512 LACA FPA is shown in Fig. 26. This imager can be operated at 75 frames/s with a 5 MHz horizontal clock. For operation with f/1.8 optics NEΔT of 1.0K was measured [55]. Most recent data for the 512 x 512 LACA FPA gives maximum data rate of 20 MHz/pixel, 75 frames/s, saturation charge (Q_{max}) of 4 x 10^5 electrons/pixel, a readout noise for 80K background of 30 rms electrons/pixel, and uniformity (wide aperature) of > 99.5% rms.

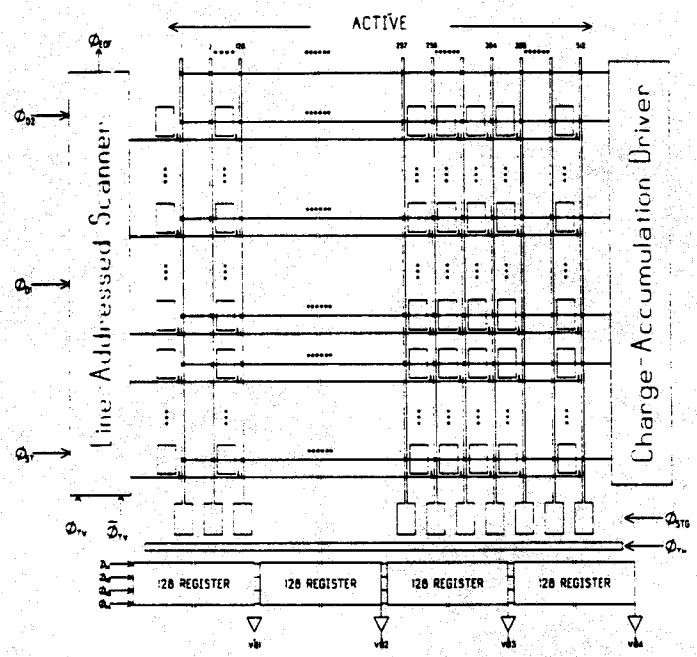

Fig. 23. Block diagram of the 512 x 512 LACA FPA (Reticon-1989).

5.3.8 MOS FPAs

The SBD FPAs with MOS readout multiplexers can be designed for column readout operation (Fig. 24) or for row readout operation (Fig. 25). The first 64 x 64 MOS SBD FPA has been constructed by Mitsubishi with the column readout operation [18]. However, a SBD FPA with row-readout MOS multiplexer is expected to be capable of lower readout noise than the column-readout MOS FPA. Relatively low readout noise of about 300 rms electrons/pixel was demonstrated in a visible MOS FPA with a row-readout design operated with an off-chip current amplifier [41]. This imager was referred to as the Transversal Signal Line (TSL) imager. It might be interesting to note, however, that, as illustrated in Fig. 25, the row-readout MOS FPA design requires an output readout with correlated double sampling to remove the reset noise at the output sensing mode [31].

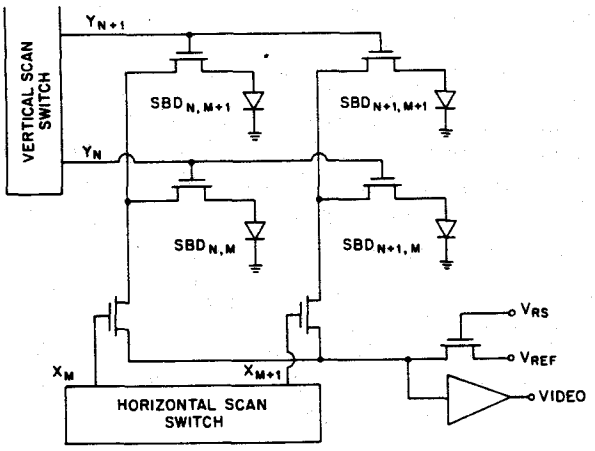

Fig. 24. SBD FPA with column-readout MOS multiplexer.

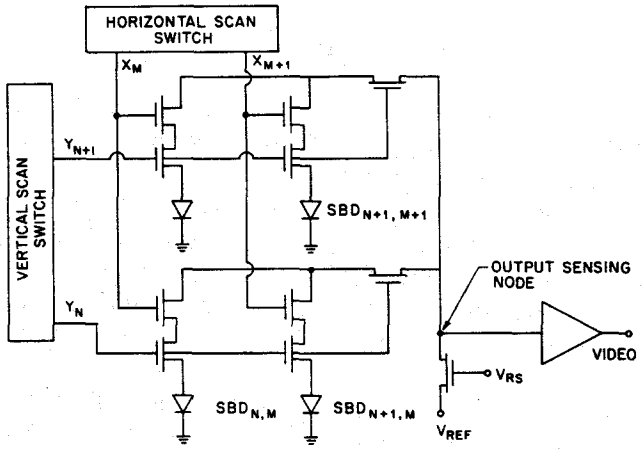

Fig. 25. SBD FPA with row-readout MOS multiplexer.

In general, the MOS SBD FPAs have the advantage of large fill factor, large Q_{max} that is limited only to SBD capacitance and voltage, and are suitable for construction of high resolution imagers. For example, using VLSI (1.25 μm) design rules, a 60% fill factor can be obtained for 30-μm x 30-μm pixels. Another unique advantage of SBD FPAs with MOS multiplexer is that they can be operated at considerably lower temperature (as low as 40K) than SBD FPAs with buried-channel CCD registers. The major disadvantage of the SBD FPAs with MOS multiplexer is a higher readout noise than for the case of the CCD multiplexer.

A low-noise 640 x 480 MOS FPA was announced by the David Sarnoff Research Center with 25-μm x 24-μm pixels and 38% fill factor for 1.5-μm process design rules [63]. This FPA has a low-noise x-y addressable readout multiplexer (see Fig. 26) with two MOS switches per SBDs, an MOS source follower at the output of each row with 8:1 multiplexer output sense line and an on-chip correlated-double-sampling (CDS) output amplifier. The estimated total MOS multiplexer readout noise for this FPA is estimated to be < 100 rms electrons/pixel.

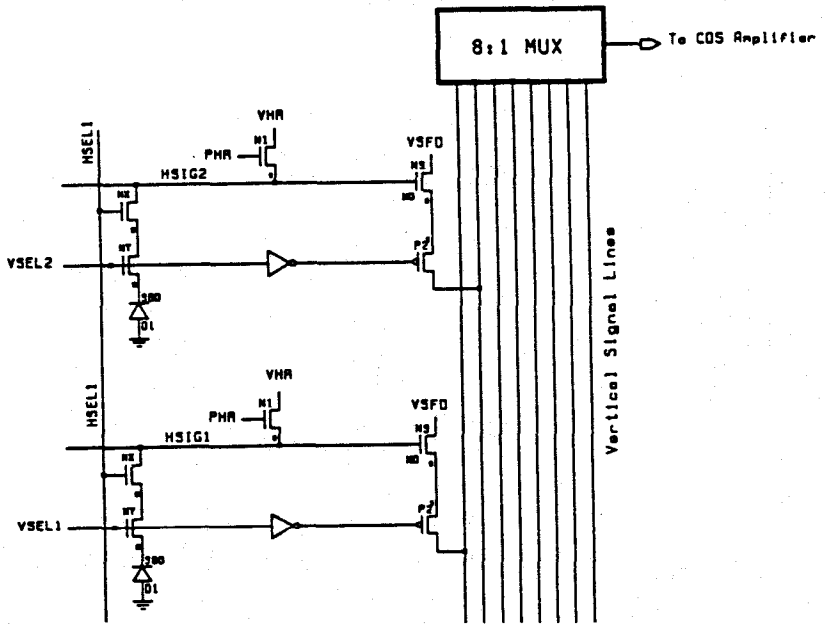

Fig. 26. Low-noise MOS readout multiplexer of the Sarnoff 640 x 480 MOS FPA.

5.3.9 Hughes 400 x 244 Hybrid FPA

A family of hybrid FPAs was reported by Hughes Aircraft Co. in a form of a 256 x 256, 400 x 244, and 640 x 488 arrays of PtSi SBDs connected by indium bumps to a silicon readout multiplexer [37, 54]. A high fill factor can be achieved with the hybrid FPAs by close spacing of PtSi SBDs without guard rings [43]. The 400 x 244 hybrid FPA was constructed using 2-μm design rules with 24-μm x 24-μm pixels and 84% fill factor for operation with maximum charge of 7.5 x 10^5 electrons/pixel [54]. The construction of the hybrid FPA with PtSi SBDs is illustrated in Fig. 27. The silicon MOS readout multiplexer of the 400 x 244 hybrid FPA was designed for operation with direct integration using x-y addressable switches integrators for operation with correlated double sampling (CDS) illustrated in Fig. 28, 29 and 30 [37, 54]. Operation of this FPA in the CSD mode required a frame memory for storing the "reset level" readout (point 1A in Fig. 26) to be subtracted (at the end of frame 1) from the "signal level" readout (point 1B). However, the hybrid FPA has also been operated in a simpler "delta-reset" mode, in which case the change in potential between points 1B and 2A in Fig. 30 is measured before and after SBD reset. For operation with an optical integration time of 16.7 ms (60 frames/s) and f/1.8 telescope, the 400 x 244 hybrid FPA was reported to have NEΔT of 0.08K for 300-K background [54].

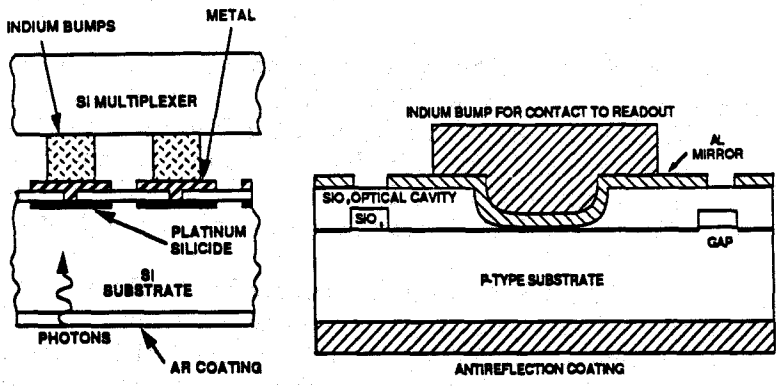

Fig. 27. Cross-sectional views illustrating the construction of hybrid FPA with closely-spaced PtSi SBDs without guard rings.

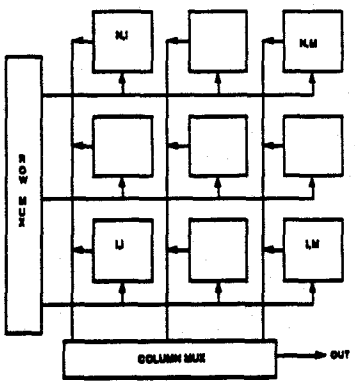

Fig. 28. Block diagram of hybrid SBD FPA with x-y addressable MOS direct readout.

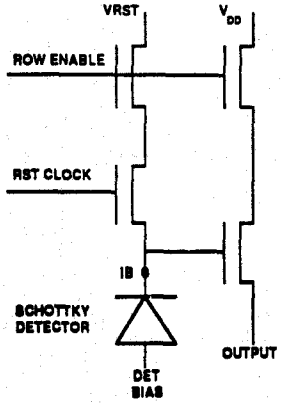

Fig. 29. Schematic of the pixel cell of the hybrid FPA.

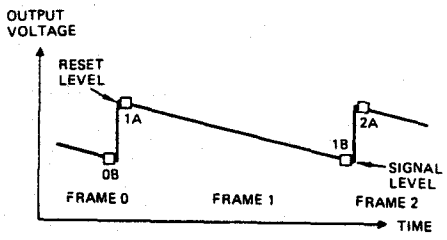

Fig. 30. Output signal sampling in hybrid FPA.

5.3.10 Direct Schottky Injection FPA

A Direct Schottky Injection (DSI) imager structure represents an approach for the FPA with 100% fill factor [64, 65]. The DSI structure consists of continuous Schottky-barrier-detector surface on one side of a thinned (~ 20-μm thick) silicon substrate and p-type buried-channel CCD readout in an N-well on the other side. The feasibility of the DSI concept was demonstrated at the David Sarnoff Research Center with a 128 x 128 DSI FPA with 50-μm x 50-μm pixels and p-channel IT-CCD readout multiplexer [64]. In addition to a 100% fill factor, the DSI construction provides large charge handling capacity and high-density pixel design at the cost of a reduction of the SBD responsivity by about a factor of 2 and somewhat more complex device process requiring thinning of the back surface of the completed silicon wafer to about 20 μm before the deposition of platinum and the formation of the PtSi Schottky-barrier surface.

5.3.11 IT-CCD FPA with Silicon Cylindrical Lens Array

The fill factor of an IT-CCD FPA can be improved by a refractive or diffractive lens array formed on the back-side of the appropriately thinned silicon substrate. The concept of a refractive silicon cylindrical array was originally demonstrated at the David Sarnoff Research Center by H. G. Erhardt with a 32 x 63 and 64 x 128 IT-CCD FPAs [74].

5.3.12 FISA FPAs

Still another approach for the construction of high fill factor SBD FPAs is the "Fully Integrated Schottky Array" (FISA) concept recently proposed and demonstrated at the University of New South Wales, Kensington, Australia [60, 75]. The FISA imager is frame transfer CCD (FT-CCD) array in the form of infrared sensitive Schottky CCD gate formed on p-type buried-channel implant layer on an N-type silicon substrate. A novel technique for patterning of submicron gaps between the silicide CCD gates was recently described by Theden et al. [60]. In this construction low barrier silicide gates are used for the photosensitive FT-CCD area and infrared-insensitive high barrier silicide gates for the storage and output sections of the imager.

6.0 SUMMARY OF CHARACTERISTICS OF STARING SBD FPAs

The characteristics of the state-of-the-art PtSi SBD FPAs are summarized in Table 3. In addition to the pixel size and fill factor given for these arrays in Table 1, Table 4 also indicates the process design rules used, maximum charge signal, Q_{max}, and the reported noise equivalent temperature, NEΔT, for operation with a given f/# of the optics of the cold shield. The Sarnoff 320 x 244 IT-CCD FPA [48] has the largest Q_{max} of 1.4×10^6 electrons/pixels and is capable of thermal imaging at about 300K background with the lowest NEΔT of about 0.04K. The Sarnoff FPAs are also characterized by SBD dark current density at 77K in the range of 1 to 4 nA/cm^2 for SBD bias of about 4V [48]. Similar dark current was also reported by the Fairchild 512 x 488 IT-CCD FPAs [51]. The highest resolution with the largest fill-factor of 54% for a monolithic FPA was reported by Kodak for the uninterlaced 640 x 486 IT-CCD FPA.

However, the largest fill factor of 84% was achieved by Hughes with the 400 x 244 hybrid FPA [54]. Depending on the readout mode, the hybrid FPA with switched MOS integrators is also capable of very low multiplexer readout noise in the range of 40 to 100 rms electrons/pixel. The most widely commercially available SBD IR TV camera system is provided by Mitsubishi with the 512 x 512 CSD FPA (see thermal imaging in Fig. 22) [56].

Very good spatial uniformity was achieved by most reported FPAs with PtSi SBDs. The spatial non-uniformity or fixed pattern noise (FPN) in the range of 1 to 3% rms was reported for non-corrected video output of PtSi FPAs [21, 48, 54, 61, 66]. Therefore, excellent quality thermal imaging can be achieved with these FPAs for thermal imaging with one-point uniformity correction [9, 17, 19, 21, 35, 48]. In fact as illustrated in Fig. 14, some recent 320 x 244 PtSi FPAs made at the David Sarnoff Research Center have good enough uniformity to produce useful infrared imaging without any uniformity correction.

Table 3. State-of-the-Art Staring PtSi FPAs.

Type of FPA	Pixel Size (μm^2)	Fill Factor (%)	Design Rules (μm)	Qmax x 10^5 (e^-/p)	NEΔT (K)	f/#	Year	Company
320 x 244 IT-CCD	40 x 40	44	2.0	1.4	0.04	1.4	1988	Sarnoff
324 x 487 IT-CCD	42 x 21	42	1.5	0.2 - 0.3	0.10	1.2	1988	NEC
512 x 488 IT-CCD	31.5 x 25	36	1.8	0.55	0.07	1.8	1989	Loral Fairchild
640 x 486 IT-CCD 2ø not interlaced	25 x 25	54	1.2	0.22	0.15	2.8	1990	Kodak
256 x 256 IT-CCD Meander-Channel Al-F.P. not interlaced	40 x 40	52	3.0	1.2	0.10	2.4	1990	Ford
512 x 512 CSD	26 x 20	39	2.0	0.7 @ 4V 1.4 @ 11V	0.10 0.07	1.5 1.2	1987 1989	Mitsubishi
512 x 512 LACA	30 x 30	54	2.5	0.4	---	1.8	1989	Reticon
400 x 244 Hybrid	24 x 24	84	2.0	0.75	0.08	1.8	1990	Hughes

Finally, as illustrated in Fig. 15, the PtSi FPA can be operated to give shot-noise-limited performance with a noise floor of about 100 rms electrons/pixel [48]. Recent data also shows that the PtSi FPA does not exhibit any 1/f SBD noise [68].

7.0 CONCLUSIONS

Infrared image sensors with PtSi Schottky-barrier detectors (SBDs) are becoming accepted as a IR technology for many SWIR and MWIR applications. These FPAs are fabricated by a well established silicon process VLSI process that assures low production cost for large volume, excellent infrared response uniformity, and offer at this time, probably the most promising IR technology for very high-resolution and large-area IR imagers.

Scanning PtSi FPAs with up to 4 x 4096 elements and 2048 x 16 TDI elements were developed for space-borne remote sensing applications. High-resolution staring PtSi FPAs were developed with up to 512 x 512 and 640 x 486 elements. In a year or two monolithic 1024 x 1024 PtSi FPAs are expected to be available for remote sensing and machine vision applications.

Very good thermal imaging near 300K-background was demonstrated with noise equivalent temperature (NEΔT) of 0.04K to 0.15K for staring PtSi FPAs with 320 x 244 elements to 640 x 486 elements for operation at a temperature of 77K and 30 frames/s with f/1.4 to f/2.8 optics.

FPAs with IrSi SBDs with cut-off wavelength up to 10 μm were demonstrated for operation in the LWIR band at a temperature of about 45K.

ACKNOWLEDGEMENT

The author would like to express his appreciation to many colleagues for providing illustrations and preprints of their paper for this review. The author would also like to take this opportunity to thank his colleagues from David Sarnoff Research Center for their contributions to this paper and H. R. Gilmartin for proofreading and Lisa Pullen for typing this manuscript.

8.0 REFERENCES

1. F. D. Shepherd and A. C. Yang, "Silicon Schottky Retinas for Infrared Imaging," Int. Electron Devices Meet., Tech. Dig., pp. 310-313, 1973.
2. E. S. Kohn, S. A. Roosild, F. D. Shepherd, and A. C. Yang, "Infrared Imaging with Monolithic, CCD-Addressed Schottky-Barrier Detector Arrays, Theoretical and Experimental Results," Presented at Int. Conf. on Application on CCD's, Oct. 29-31, 1975.
3. B. R. Capone, L. H. Skolnik, R. W. Taylor, F. D. Shepherd, S. A. Roosild, W. Ewing, W. F. Kosonocky, and E. S. Kohn, "Evaluation of a Schottky IRCCD Staring Mosaic Focal Plane," presented at 22nd Int. Tech. Symp. Society of Photo-Optical Instrumentation Engineers, San Diego, CA, Aug. 28-29, 1978.
4. W. F. Kosonocky, E. S. Kohn, F. V. Shallcross, D. J. Sauer, F. D. Shepherd, L. H. Skolnik, R. W. Taylor, B. R. Capone, and S. A. Roosild, "Platinum-Silicide Schottky-Barrier IR-CCD Image Sensors," Int. Conf. on Application of CCD's, pp. 2-7-2-38, Oct. 25-27, 1978.
5. F. D. Shepherd, R. W. Taylor, L. H. Skolnik, B. R. Capone, S. A. Roosild, W. F. Kosonocky, and E. S. Kohn, "Schottky IRCCD Thermal Imaging," Adv. Electron. Electron Phys., 7th Symp. Photo-Electronic Image Devices, Vol. 22, pp. 495-512, 1979.
6. R. W. Taylor, L. H. Skolnik, B. R. Capone, E. Ewing, F. D. Shepherd, S. A. Roosild, B. Cochrun, M. Cantella, J. Klein, and W. F. Kosonocky, "Improved Platinum Silicide IRCCD Focal Plane," Presented at SPIE's Tech. Symp. Advances in Focal Plane Technology, Los Angeles, CA, Feb. 4-5, 1980.
7. W. F. Kosonocky, H. G. Erhardt, G. M. Meray, F. V. Shallcross, H. A. Elabd, M. J. Cantella, J. Klein, L. H. Skolnik, B. R. Capone, R. W. Taylor, W. Ewing, F. D. Shepherd, and S. Roosild, "Advances in Platinum-Silicide Schottky-Barrier IR-CCD Image Sensors," SPIE IR-Image Sensor Technol., Vol. 225, pp. 69-71, 1980.
8. M. Kimata, M. Denda, T. Fukumoto, N. Tsubouchi, S. Uematsu, H. Shibata, T. Higuchi, T. Saheki, R. Tsunoda, and T. Kanno, "Platinum Silicide Schottky-Barrier IR-CCD Image Sensors," J. Proc. 13th Conf. Solid State Devices, (Tokyo, Japan), pp. 231-235, 1981.
9. W. F. Kosonocky, H. Elabd, H. G. Erhardt, F. V. Shallcross, T. Villani, G. Meray, M. J. Cantella, J. Klein, and N. Roberts, "64 x 128-Element High-Performance PtSi IR-CCD Image Sensor," Presented at IEDM, Washington, DC, Dec. 7, 1981.
10. H. Elabd, T. Villani, and W. F. Kosonocky, "Palladium-Silicide Schottky-Barrier IR-CCD for SWIR Applications at Intermediate Temperatures," IEEE Trans. Electron Devices Lett., Vol. EDL-3, pp. 89-90, Apr. 1982.
11. W. F. Kosonocky, H. Elabd, H. G. Erhardt, F. V. Shallcross, G. Meray, T. S. Villani, J. V. Groppe, R. Miller, V. L. Frantz, M. J. Cantella, J. Klein, and N. Roberts, "Design and Performance of 64 x 128-element PtSi Schottky-Barrier IR-CCD Focal Plane Array," Presented at SPIE Tech. Symp. East, Arlington, VA, May 3-7, 1982.
12. H. Elabd, T. S. Villani, and J. R. Tower, "High Density Schottky-Barrier IRCCD Sensors for SWIR Applications at Intermediate Temperature," SPIE Tech. Symp. East, Arlington, VA, May 3-7, 1982.
13. H. Elabd, and W. F. Kosonocky, "Theory and Measurements of Photoresponse for Thin-Film Pd_2Si and PtSi Infrared Schottky-Barrier Detectors with Optical Cavity," RCA Review, Vol. 44, Dec. 1982.
14. M. Kimata, M. Denda, N. Yutani, N. Tsubouchi, H. Shibata, H. Kurebayashi, S. Uematsu, "A 256 x 256-Element Si Monolithic IR-CCD Imager," 1983 ISSCC Dig. Tech. Papers, pp. 254-255.
15. T. Tanikawa, Y. Ito, and A. Shimonashi, "A PtSi Schottky-Barrier Area Imager with Meander-Channel CCD Readout Registers," IEEE Trans. Electron Device Lett., Vol. EDL-4, No. 3, pp. 66-67, Mar. 1983.
16. W. F. Kosonocky, and H. Elabd, "Schottky-Barrier Infrared Charge-Coupled Device Focal Plane Arrays," 27th SPIE International Technical Symposium, San Diego, CA, Aug. 23-26, 1983 (SPIE Vol. 443).

17. W. S. Ewing, "Silicide Mosaic Array Compensation," SPIE Proc., Vol. 409, 1983.
18. M. Denda, M. Kimata, N. Yutani, N. Tsubouchi, and S. Uematsu, "A PtSi Schottky-Barrier Infrared MOS Area Imager with Large Fill Factor," Presented at Int. Electron Device Meet., Washington, DC, Dec. 5-7, 1983.
19. F. D. Shepherd, "Recent Advances in Platinum Silicide Infrared Focal Plane Arrays," 1984 IEDM Tech. Digest, San Francisco, CA, Dec. 9-12, 1984, pp. 370-372.
20. J. Mooney and J. Silverman, "The Theory of Hot-Electron Photoemission in Schottky-Barrier IR Detectors," IEEE Trans. Electron Devices, Vol. ED-32, No. 1, pp. 33-39, 1985.
21. W. F. Kosonocky, F. V. Shallcross, T. S. Villani and J. V. Groppe, "160 x 244 Element PtSi Schottky-Barrier IR-CCD Image Sensor," IEEE Trans. Electron Devices, Vol. ED-32, No. 8, pp. 1564-1573, August, 1985.
22. J. R. Tower, L. E. Pellon, B. M. McCarthy, H. Elabd, A. G. Moldovan, W. F. Kosonocky, J. E. Kalshoven, and D. Tom, "Shortwave Infrared 512 x 2 Line Sensors for Earth Resources Applications," IEEE Trans. Electron Devices, Vol. ED-32, pp. 1574-1583, August, 1985.
23. M. Kimata, M. Denda, N. Yutani, S. Iwade, and N. Tsubouchi, "A 512 x 512 Element PtSi Schottky-Barrier Infrared Image Sensor," 1987 ISSCC Digest of Tech. Papers, New York, NY, Feb. 25-27, 1987, pp. 110-111.
24. L. R. Hudson, H-F Tseng, W-L Wang, "PtSi Infrared Area Array Utilizing MOS/CTD Readout," SPIE Proceedings, Vol. 819-22, San Diego, CA, August 18-20, 1987.
25. L. R. Hudson, H-F Tseng, W-L Wang, G. P. Weckler, "Schottky-Barrier Infrared Focal Plane Array for Spectroscopic Applications," Optical Engineering, Vol. 26, No. 3, pp. 216-222, March, 1987.
26. H. G. Grof, M. Koniger, L. Senatori, "Schottky-Barrier IR-CCD Focal Plane Arrays," IEE Conf. Publication, No. 268, p. 1-6, (1986), Conference on Advanced Infrared Detectors and Systems, 3-5 June, 1986, London.
27. M. Denda, M. Kimata, S. Iwade, N. Yutani, T. Kondo, and N. Tsubouchi, "4 x 4096-Element SWIR Multispectral Focal Plane Array," SPIE Proceedings, Vol. 819-24, San Diego, CA, Aug. 18, 1987.
28. P. W. Pellegrini, A. Golubovic, C. E. Ludington, and M. M. Weeks, "IrSi Schottky-Barrier Diodes for Infrared Systems," 1982-IEDM Technical Digest, pp. 157-159, Dec. 1982.
29. P. W. Pellegrini, A. Golubovic, and C. E. Ludington, "A Comparison of Iridium Silicide and Platinum Silicide Photodiodes," SPIE Vol. 782, Infrared Sensors and Sensor Fusion, Orlando, FL, May, 1987, pp. 93-98.
30. N. Yutani, M. Kimata, M. Denda, S. Iwade, and N. Tsubouchi, "IrSi Schottky-Barrier Infrared Image Sensor," 1987-IEDM Technical Digest, pp. 124-127, December, 1987.
31. W. F. Kosonocky and G. W. Hughes, "High Fill Factor Silicide Monolithic Arrays," SPIE Vol. 782, Infrared Sensors and Sensor Fusion, Orlando, FL, May, 1987, pp.
32. P. Pellegrini, M. Weeks, C. Ludington, "New 6.5 μm Photodiodes for Schottky-Barrier Array Applications," SPIE Vol. 311 Mosaic Focal Plane Methodologies II (1981), pp. 24-29.
33. W. F. Kosonocky and H. Elabd, "Schottky-Barrier Diode Radiant Energy Detector with Extended Longer Wavelength Response," U.S. Patent No. 4,544,939, October 1, 1985.
34. J. M. Mooney, J. Silverman, and M. M. Weeks, "PtSi Internal Photoemission: Theory and Experiment" SPIE Vol. 782, Infrared Sensors and Sensor Fusion (1987), pp. 99-107.
35. M. Kimata, M. Denda, N. Yutani, S. Iwade, and N. Tsubouchi, "A 512 x 512-Element PtSi Schottky-Barrier Infrared Image Sensor," IEEE J. Solid-State Circuits, Vol. SC-22, No. 6, December, 1987, pp. 1124-1129.
36. M. Koniger, W. Platz, L. Senatori, "128 x 64 Element Schottky Barrier IR-CCD Focal Plane Array," SPIE 865, Focal Plane Arrays: Technologies and Applications, Cannes, France, 16-20 November, 1987.
37. R. Aquilera, "256 x 256 Hybrid Schottky Focal Plane Arrays," SPIE Vol. 782 Infrared Sensors and Fusion, Orlando, FL, May, 1987, pp. 108-113.

38. M. Denda, M. Kimata, S. Iwade, N. Yutani, T. Kondo, and N. Tsubouchi, "Multispectral Band Schottky-Barrier IRCCD for Remote-Sensing Applications," SPIE Proceedings Vol. 1308-12, Orlando, FL, April, 1990 (this Issue).
39. W. F. Kosonocky, F. V. Shallcross, T. S. Villani, G. Meray, and J. V. Groppe, "A 320 x 244-Element IR-CCD Imager with PtSi Schottky-Barrier Detectors," IRIS, August 16-18, 1988.
40. W. F. Kosonocky and F. V. Shallcross, "Method of Making a Charge-Coupled Device Imager which Includes an Array of Schottky-Barrier Detectors," U.S. Patent No. 4,548,671, October 22, 1985.
41. S. Nishizawa, T. Miyazawa, M. Uehara, A. Hyasaka, I. Takemoto, and M. Ashikawa, "A New, Transversal Signal Line (TSL) Type Solid State Imager," Proceedings of SPSE's Conference and Exhibition on Electronic Imaging, 26th Fall Symposium, Oct. 13-17, 1986, Crystal City, Arlington, VA, pp. 42-47.
42. B. Tsaur, M. M. Weeks, P. W. Pellegrini, "Pt-Ir Silicide Schottky-Barrier IR Detectors," IEEE Electron Device Letters, Vol. 9, No. 2, February, 1988, pp. 100-102.
43. F. D. Shepherd, P. W. Pellegrini, C. E. Ludington, M. M. Weeks, "Self-Guarding Schottky Barrier Infrared Detector Array," U.S. Patent No. 4,531,055, July 23, 1985.
44. B.-Y. Tsaur, M. M. Weeks, R. Trubiano, P. W. Pellegrini, and T.-R. Yew, "IrSi Schottky-Barrier Infrared Detectors with 10-μm Cutoff Wavelength," IEEE Elect. Device Letters, Vol. 9, No. 12, Dec., 1988, pp. 650-653.
45. B.-Y. Tsaur, M. J. McNutt, R. A. Bredthauer, R. B. Mattson, "128 x 128-Element IrSi Schottky-Barrier Focal Plane Arrays for Long-Wavelength Infrared Imaging," IEEE Electron Device Letters, Vol. 10, No. 8, August, 1989, pp. 361-363.
46. B.-Y. Tsaur, C. K. Chen, and J.-P. Mattia, "PtSi Schottky-Barrier Focal Plane Arrays for Multispectral Imaging in Ultraviolet, Visible, and Infrared Spectral Bands," IEEE Electron Device Letters, Vol. 11, No. 4, April, 1990, pp. 162-164.
47. J. Kurianski, J. Van Damme, J. Vermeiren, K. Malx, and C. Claeys, "Nickel Silicide Silicide Schottky Barrier Detectors for Short Wavelength Infrared Applications," SPIE Proceedings, Vol. 1308-0, Orlando, FL, April, 1990, (This issue).
48. T. S. Villani, W. F. Kosonocky, F. V. Shallcross, J. V. Groppe, G. M. Meray, J. J. O'Neill, III, and B. J. Esposito, "Construction and Performance of a 320 x 244-Element IR-CCD Imager with PtSi SBDs," SPIE Vol. 1107-01, March, 1989.
49. K. Konuma, N. Teranishi, S. Tohyama, K. Masubuchi, S. Yamagata, T. Tanaka, E. Oda, Y. Moriyama, N. Takada, and N. Yoshioka, "324 x 487 Schottky-Barrier Infrared Imager," IEEE Trans. Electron Devices, Vol. 37, No. 3, March, 1990, pp. 629-635.
50. R. H. Dyck, J. S. Kim, Y. Abedini, H. Elabd, W. G. Petro, K. K. Shah, J. A. Lehan, J. Chin, J. Wong, H. L. Balopole, J. C. Holland, and T. A. Pletcher, "A 244 x 290 Element PtSi Imager Built with Mature CCD Production Technology," SPIE Proceedings Vol. 924-09, Orlando, April, 1988.
51. H. Elabd, Y. Abedini, J. Kim, M. Shih, J. Chin, K. Shah, J. Chen, F. Nicol, W. Petro, J. Lehan, M. Duron, M. Manderson, H. Balopole, P. Coyle, P. Cheng, W. Shieh, "488 x 512 and 244 x 256-Element Monolithic PtSi Schottky IR Focal Plane Arrays," SPIE Vol. 1107-29, Aerospace Sensor Symposium, March, 1989, Orlando, FL.
52. E. T. Nelson, K. Y. Wong, S. Yoshizumi, D. Rockafellow, W. DesJardin, M. Elzinga, J. P. Lavine, T. J. Tredwell, R. P. Khosla, P. Sorlie, B. Howe, S. Brickman, S. Refermat, "Wide Field of View PtSi Infrared Focal Plane Array," SPIE Proceeding, Vol. 1308, Orlando, FL, April, 1990 (This issue).
53. M. T. Daigle, D. Colvin, E. T. Nelson, S. Brickman, K. Wong, S. Yoshizumi, M. Elzinga, P. Sorlie, D. Rockafellow, P. Travers, R. Avel, "High Resolution 2048 x 16 TDI PtSi IR Imaging CCD," SPIE Proceedings, Vol. 1308, Orlando, FL, April, 1990 (This issue).
54. J. Edwards, J. Gates, H. Altin-Mees, W. Connelly, A. Thompson, "244 x 400 Element Hybrid Platinum Silicide Schottky Focal Plane Array," SPIE Proceedings, Vol. 1308-9, Orlando, FL, April, 1990 (This issue).

55. W.-L. Wang, R. Winzenread, B. Nguyen, J. J. Murrin, R. L. Trubiano, "High Fill Factor 512 x 512 PtSi Focal Plane Array," SPIE Proceedings, Vol. 1161-12, San Diego, CA, 1989.
56. S. Tujino, T. Miyoshi, M. Yokoh, T. Kitahara, "Mitsubishi Thermal Imager Using the 512 x 512 PtSi Focal Plane Array," SPIE Proceedings, Vol. 1157-17, San Diego, 1989.
57. M. Kimata, M. Denda, and N. Tsubouchi, "High Density Schottky-Barrier Infrared Image Sensor," Journal of Sensor and Actuators, Dec., 1989.
58. M. J. McNutt, "Monolithic Schottky Barrier Focal Plane Arrays with High Fill Factors," SPIE Proceedings, Vol. 1308, Orlando, FL, April, 1990, (This issue).
59. N. Teranishi, H. Harada, T. Tanaka, K. Arai, "A High Resolution Linear IRCCD Image Sensor," Trans. IECE of Japan, Vol. E69, No. 4, April, 1986, pp. 274-276.
60. J. M. Kurianski, U. Theden, M. A. Green, and W. V. Storey, "Novel 896-Element Infrared Schottky Detector Line Array," IEEE Electron Device Letters, Vol. 9, No. 9, Sept. 1988, pp. 436-438.
61. R. Maddox, S. Burt, "High Performance PtSi Linear and Area Focal Plane Arrays," SPIE Proceedings, Vol. 1308-36, Orlando, FL, April, 1990 (This issue).
62. W. F. Kosonocky, "Infrared Image Sensors with Schottky-Barrier Detectors," SPIE Proceedings Vol. 869, Cannes, France, November, 1987, pp. 90-106.
63. D. J. Sauer, F. L. Hsueh, F. V. Shallcross, G. M. Meray, T. S. Villani, "640 x 480 Element PtSi IR Sensor with Low Noise MOS X-Y Addressable Readout Multiplexer," SPIE Proceedings Vol. 1308-07, Orlando, FL, April, 1990 (This issue).
64. W. F. Kosonocky, T. S. Villani, F. V. Shallcross, G. M. Meray, and J. J. O'Neill, III, "A Schottky-Barrier Image Sensor with 100% Fill Factor," SPIE Proceedings, Vol. 1308-05, Orlando, FL, April, 1990 (This issue).
65. W. F. Kosonocky, U. S. Patent No. 4,774,557, "Back-Illuminated Semiconductor Imager with Charge Transfer Device on Frame Surface Well Structure," Sept. 27, 1988.
66. J. E. Marguia and W. S. Ewing, "Statistical Characterization of a Large PtSi Focal Plane Array," SPIE Vol. 782, Infrared Sensors and Sensor Fusion (1987), pp. 121-128.
67. F. D. Shepherd and J. M. Mooney, "Design Considerations for IR Staring-Mode Cameras," SPIE Vol. 762 Electro-Optical Imaging Systems Integration (1987), pp. 35-50.
68. J. M. Mooney, "1/f Measurements on PtSi Focal Plane Arrays," SPIE Proceedings Vol. 1308-10, Orlando, FL, April, 1990 (This issue).
69. R. J. Archer and J. Cohen, "Schottky-Barrier Monolithic Detector Having Ultrathin Metal Layer," U.S. Patent 3,757,123, September 4, 1973.
70. J. Cohen, J. Vilms and R. J. Archer, "Investigation of Semiconductor Schottky Barriers for Optical Detection and Cathodic Emission," Air Force Cambridge Research Labs. Report No. 68-0651 (1968).
71. S. M. Sze, "Physics of Semiconductors," Second Edition, Wiley-Interscience, p. 264.
72. D. L. Losee, J. P. Lavine, U. S. Patent No. 4,613,402, "Method of Making Edge-Align Implants and Electrodes Therefore," Sept. 23, 1986.
73. M. J. McNutt, "Edge Leakage Control in Platinum-Silicide Schottky-Barrier Diodes Used for Infrared Detection," IEEE Electron Device Letters, 9, August, 1989, pp. 394-396.
74. H. G. Erhardt, et al., "Silicon Cylindrical Lens Array for Improved Photoresponse in Focal Plane Array," SPIE Vol. 501, (1984), pp. 165-172.
75. U. Theden, M. A. Green, J. W. V. Storey, J. M. Kurianski, "The Fully Integrated Schottky Array," SPIE Proceeding, Vol. 1308-34, Orlando, FL, April, 1990 (This issue).
76. H. Elabd and W. F. Kosonocky, U. S. Patent # 4,638,345, "IR Imaging Array and Method of Making Same," Jan. 20, 1987.